Structural and Multidisciplinary Optimization (2021) 64:113–124
https://doi.org/10.1007/s00158-021-02862-x

RESEARCH PAPER

Phononic band gap optimization in truss-like cellular structures using smooth P-norm approximations

Leonel Quinteros[1,2] · Viviana Meruane[1,2] · Eduardo Lenz Cardoso[3]

Received: 6 April 2020 / Revised: 3 September 2020 / Accepted: 19 January 2021 / Published online: 19 February 2021

Abstract

The emergence of additive manufacturing and the advances in structural optimization have boosted the development of tailored cellular materials. These modern materials with complex architectures show higher structural efficiency when compared to traditional materials. In particular, truss-like cellular structures show great potential to be applied in lightweight applications due to their large strength/stiffness to mass ratio. Besides lightweight, these materials may exhibit incredible vibration isolation properties known as phononic band gaps. The present investigation addresses the topology optimization of two-dimensional (2D) truss-like cellular structures. The formulation aims to find the optimal geometrical and mechanical properties of each truss element to create a material exhibiting outstanding vibration (elastic wave) isolation at a certain frequency range (band gap). A new method to handle the non-differentiation of repeated eigenvalues, as well as mode switching, is proposed, where P-norms are used to create continuous approximation for extreme frequency values for all wave vectors of the band diagram. Results show that the proposed formulation is effective and avoids convergence problems associated to mode switching and to repeated eigenvalues.

Keywords Truss-like · Phononic band gap · Optimization · Tailored cellular materials

1 Introduction

The development of additive manufacturing technologies has allowed the fabrication of cellular materials with increasingly complex architectures (Schaedler and Carter 2016). Furthermore, recent advances in topology optimization enable the optimization of tailored materials to meet desired objectives, such as lightweight and high strength and stiffness. Indeed, it has been demonstrated that lattice-based materials can deliver an almost ideal relationship between stiffness, strength, and density (Cheung and Gershenfeld 2013), making them attractive in low-weight applications, such as aircraft design (Cramer et al. 2019).

Tailored cellular materials not only show interesting static properties but can also be used to manipulate the propagation of mechanical waves as the case of phononic band gaps (Liebold-Ribeiro and Körner 2014). Phononic materials can mitigate wave propagation in a medium at a certain frequency range. Due to this behavior, these kinds of materials have been exhaustively investigated in recent years (Hussein et al. 2014).

Jensen (2003) showed that truss-like periodic structures present band gaps that prevent elastic waves of certain frequencies from propagating. It was also shown that wave guides are obtained by replacing the periodic structure with a homogeneous structure in certain paths. Ruzzene and Scarpa (2005) investigated the band gap and the directional characteristics of honeycomb and auxetic lattices. The lattices consist of a frame-type structure composed of an array of struts rigidly connected. The authors demonstrated that the band gap is highly sensitive to the internal angle of the honeycomb and auxetic lattices. Liebold-Ribeiro and Körner (2014) studied the band gap behavior of two-dimensional periodic cellular materials with respect to two

Responsible Editor: Gengdong Cheng

✉ Leonel Quinteros
Leonel.quinteros@ug.uchile.cl

1 Department of Mechanical Engineering, Universidad de Chile, Beauchef 851, Santiago, Chile

2 Millennium Nucleus on Smart Soft Mechanical Materials, Beauchef 851, Santiago, Chile

3 Department of Mechanical Engineering, Santa Catarina State University, Joinville, SC, Brazil

different lattice types: quadratic and hexagonal and three configurations: regular, inverse, and chiral. They did not observe band gaps in the case of regular and inverse lattice configurations, whereas the quadratic and hexagonal chiral present significant band gaps. A similar conclusion is reached by Warmuth and Körner (2015), indicating that if straight struts are replaced by bent ones (chiral) band gaps are obtained. Wang et al. (2015) studied the connection between the frequency and size of the band gaps to the lattice topology. The topology is defined by the lattice coordination number, or the average number of connections at joints. They found that in lattices with high coordination, the struts act as mechanical resonators facilitating the generation of band gaps. If the coordination number is reduced, the width of the band gap decreases until a threshold from which the band gap is no longer generated.

The investigations discussed in the previous paragraph show that if the geometrical or material properties of the struts are altered, it is possible to create band gaps. Therefore, a natural extension is the application of topology optimization techniques in the design of lattice materials with phononic band gaps. There are many investigations using topology optimization to achieve the best topologies that yield the largest band gap. Nevertheless, these investigations have been mainly focused on the design of two-dimensional solid or plate structures with one or two different materials (Yi and Youn 2016; Yi et al. 2019).

In topology optimization, a fixed design domain is discretized by a large number of elements and the material properties of each element are defined as design variables. Sigmund and Jensen (2003) were the first to apply topology optimization to optimize band gaps in phononic materials. The formulation was applied to design 2D solid structures with two base materials, and the design variables were relative densities of each element. Gazonas et al. (2006) applied genetic algorithms (GA) to find the optimal distribution of a 2D two-phase structure. In this work, binary optimization variables are used, such that the material of each element is represented as a discrete valued (zero-one) variable. A similar approach was used by Hussein et al. (2007) to maximize the sum of band gap widths across the first six bands of a 2D periodic bimaterial. Liu et al. (2014) applied a two-stage design method based on GA and the fast plane wave expansion approach to optimize the band gap of 2D solid structures. The unit cell was first divided into 20×20 pixels, and this solution was used as the initial population of the second-stage with 40×40 pixels. A specialized GA was developed by Bilal and Hussein (2011a, b) to optimize two-dimensional phononic crystals designed for in-plane and out-of-plane waves. Dong et al. (2014b) demonstrated, for 2D phononic materials, if no assumption on the symmetry of the cell is made, larger band gap widths are obtained in comparison with symmetrical cells. Diaz et al. (2005) investigated the presence of band gaps in a plane grid structure made of intersecting beams. They maximize the width of the band gap with the addition of non-structural masses placed at strategic grid locations, while the grid structure was not modified. Other studies related to grid structures are presented in Liu and Cao (2006) in which truss elements were employed and the optimum band gap was verified through experimental modal analysis. Halkjaer et al. (2005) used topology optimization to design bi-materials beams and plates with maximum band gaps. In a later work, they focused on the design of single-material plates with a maximized band gap (Halkjær et al. 2006). The optimized design was adapted to build a real structure consisting of a PolyCarbonate plate made of 10 × 10 unit cells, where the band gap was clearly visible in the frequency response function (FRF) of the structure. Vanatabe et al. (2011, 2014) applied topology optimization to maximize the band gap of a functionally graded 2D piezo-composite periodic material. They concluded that there is no need to obtain discrete zero-one solutions, since gray values can be removed by post-processing and the dispersion diagram is not significantly modified. The bidirectional evolutionary structural optimization (BESO) was first introduced in band gap maximization by Li et al. (2016). They proposed a new optimization algorithm based on BESO to design phononic band gaps in 2D structures. Yi et al. (2019) applied a gradient-based optimization algorithm to maximize the band gap width in 2D solid materials while a constraint is imposed on the central frequency of the relative band gap. Therefore, allowing to design a band gap with a maximum width taking into account a target frequency.

Considering mass or stiffness constraints some investigations have implemented multi-objective optimization strategies for phonic materials. Dong et al. (2014a) used multiple-objective GA optimization to maximize the band gap width with the minimum mass of 2D solid phononic materials, considering in-plane and out-of-plane wave modes. Using a similar multiple-objective GA optimization approach, Hedayatrasa et al. (2016) optimized the topology of a perforated solid plate in order to maximize the band gap width in conjunction with the in-plane stiffness. Hedayatrasa et al. (2016) applied multiple-objective GA optimization to maximize the band gap width and the deformation-induced band gap gradient in plate structures, with the objective of obtaining phononic plates with tunable band gaps under equibiaxial stretch. Li et al. (2016) adapted the BESO algorithm in conjunction with the homogenization method for multiple objective optimization. They maximize the band gap width and bulk or shear modulus of 2D solid materials simultaneously.

In general, heuristic optimization approaches, such as GA, are more suitable for problems with a small number of design variables. Due to the large number of function

evaluations required, the computational cost of these approaches depends strongly on the number of optimization variables. In addition, their performance is highly sensitive to the functions and parameters selected. Therefore, if gradient information is available, gradient-based optimization approaches are preferred for solving problems with a large number of design variables, even though they may converge to local optima (Yi and Youn 2016).

To apply a gradient-based optimization approach for band gap maximization, it is necessary to compute the eigenvalue sensitivities. Nevertheless, as various investigators have discussed, the sensitivity of repeated eigenvalues is a complicated issue. This is because repeated eigenvalues are not differentiable. To avoid this ploblem, Seyranian (1994) use the perturbation theory. Bensøe and Sigmund (2003) imposed a minimum distance between eigenvalues, but this implies that the eigenvalues cannot switch places (something that occurs very often while the optimization problem is running). Li and Fang (1997) make use of an entropic regularization to solve the min-max problem, which also solves the possible no differentiation of the objective function. Gravesen et al. (2011) developed a formulation where a differential function is built based on the eigenvalues. Based on that work, Torii and De Faria (2017) suggested the use of the P-norm as a continuous approximation to the extreme values of eigenvalues. This approximation is differentiable even when some of the eigenvalues used to evaluate the norm are repeated and is insensitive to mode switching.

This investigation aims to develop an ultra-light cellular truss structure with the ability to conceive large phononic band gaps. In this case, each bar has two design variables: cross-sectional area and material since if more design variables are considered in the formulation, more flexibility and wider band gaps can be achieved. To handle the non-differentiability of repeated eigenvalues as well as mode switching, the use of P-norms as smooth approximations is proposed. P-Norms are used to build a smooth and continuous objective function related to the bad gap width, from which the corresponding sensitivity analysis can be performed.

The present article is structured as follows. Section 2 presents the formulation and background of the periodic structure theory. A description of the full geometry and symmetry assumptions is made, and the Bloch theorem and the irreducible Brillouin Zone are introduced. Section 3 explains the finite element implementation, with a focus on the interpolation function of the design variables and the boundary conditions. The optimization problem is formulated in Section 4.1, while Section 4.2 presents the sensitivity analysis and the use of the P-norm to avoid the non-differentiability of repeated eigenvalues. Finally, the results are shown in Section 5 followed by the concluding remarks in Section 6.

2 Periodic structure theory

To formulate the optimization problem, it is first necessary to present some basic concepts in periodic structure theory (PST). This is necessary to impose the proper boundary conditions representing the infinite periodicity of the unit cell.

The first step is to describe the unit cell geometry. The unit cell used in this work is built as an arrangement of basic cells, which are composed of six linear truss elements and four nodes as shown in Fig. 1a. The unit cell is made of n_x and n_y basic cells, where n_x and n_y are the number of cells in the x-axis and y-axis, respectively. Figure 1b presents an example of a unit cell with $n_x = n_y = 4$. Thus, the unit cell used in this work is a simple cubic Bravais lattice and an infinite $2D$ geometry is represented by imposing periodic boundary conditions to the unit cell to represent an infinite arrangement in both the x- and y-axes.

Direct lattice vectors, denoted by $\mathbf{t}_1$ and $\mathbf{t}_2$, are defined at the unit cell as shown in Fig. 2a. This figure also describes the unit cell space, with length and width equal to L. A reciprocal cubic lattice can then be defined as shown in Fig. 2b and the reciprocal lattice vectors are denoted as $\mathbf{T}_1$ and $\mathbf{T}_2$. Vector $\mathbf{T}_1$ is perpendicular to $\mathbf{t}_2$, with a magnitude equal to $2\pi/L$, whereas $\mathbf{T}_2$ is defined as a vector perpendicular to $\mathbf{t}_1$ with a magnitude equal to $2\pi/L$. It should be noted that in Fig. 2a and b the origin of the plane is set at the center of the unit cell.

The reciprocal lattice has both up/down and left/right reflection symmetries, as well as reflection symmetry at a 45° plane. The Irreducible Brillouin Zone (IBZ) (1953) is thus defined from the independent part of the domain. The symmetry exercise also has the function of reducing the number of design variables to decrease computational cost.

The corners of the triangle defined by the IBZ are denoted as Γ, M, and X and a wave vector $\mathbf{k}$ can be defined as a closed path following the perimeter defined by these

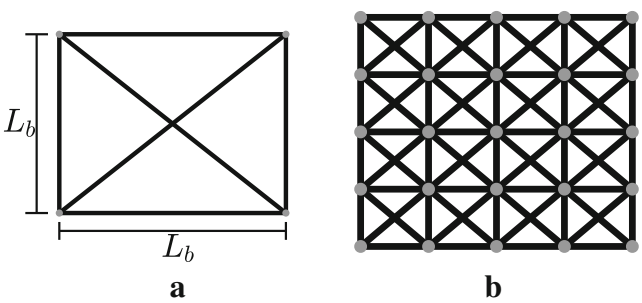

Fig. 1 Basic cell and an example of unit cell. **a** Basic cell used to build the unit cell. **b** Unit cell with $n_x = n_y = 4$

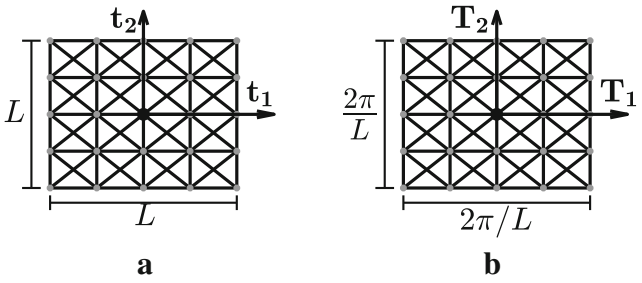

Fig. 2 Types of lattices. **a** Direct Lattice. **b** Reciprocal Lattice

corners. This path starts from Γ, passes through X and M to finally return to Γ, as shown in Fig. 3d. If the unit cell is assumed as periodic in space, Floquet-Bloch wave theory (Kittel and McEuen 1996) states that the periodic displacement in the reciprocal space is described by

$$\mathbf{u}(\mathbf{X}+\mathbf{r}) = \mathbf{u}(\mathbf{X})e^{i\mathbf{k}\cdot\mathbf{r}}, \tag{1}$$

where $\mathbf{r}$ is the periodicity of the cell, $\mathbf{u}$ is the displacement, $\mathbf{k}$ is the wave vector, and i the imaginary number. The wave vector gives the equation any possible mode of periodicity with respect to periodicity $\mathbf{r}$.

3 Finite element formulation

The unit cell is modeled by using linear truss finite elements (Bathe 2006) for each strut. Each local matrix is a function of two design variables: area of the cross section and material, specified by its Young's modulus and density. Variable x_e^A controls the effective cross-sectional area of element e and x_e^M controls the effective material of element e. The objective is to distribute two different base materials

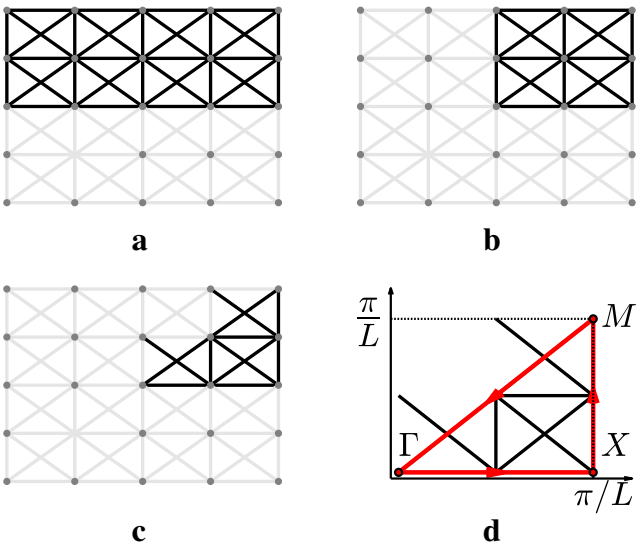

Fig. 3 Symmetries and IBZ (red) in the reciprocal lattice. **a** Up/down reection. **b** Left/right reection. **c** 45 symmetry. **d** IBZ

with properties E_1 and ρ_1 or E_2 and ρ_2. The cross-section area is interpolated between two limit values A_1 and A_2.

In this problem, x_e^A and x_e^M are defined as continuous variables in the range [0, 1]. This is performed by using an interpolation function between the range limits.The form of the interpolation function depends on the physics of the problem (Bendsøe and Sigmund 1999). Nevertheless, as stated by Sigmund et al. (2003), there is no need to use non-linear interpolation functions or to penalize intermediate values (values other than 0 or 1), since in the band gap phenomenon a large contrast between materials is favored. Therefore, a linear interpolation function is implemented here. In this case, the interpolation of a property, $P(x)$, which could be area, Young's modulus, or density ($A(x)$, $E(x)$, and $\rho(x)$), is defined as

$$P(x) = (P_2 - P_1)x + P_1, \tag{2}$$

where x represents the interpolation variable (x_e^A or x_e^M). If x equals 0, then the property will take the value P_1, whereas if x is equal to 1 the property will be equal to P_2. Therefore, if $x_e^A = 0$, the element e will be assigned with the section area A_1, and if the value is 1 instead, the section area will be A_2. The same logic applies for the materials: if the design variable $x_e^M = 0$ the element e is assigned with E_1 and ρ_1, and if the value is 1 the Young modulus is E_2 and the density is ρ_2. In this case, x_e^M controls both material properties, Young's modulus, and density.

The interpolation given in (2) is employed to define local stiffness and mass matrices as presented in (3) and (4), which assume linear shape functions.

$$\mathbf{K}_e(x_e^M, x_e^A) = \frac{E(x_e^M)A_(x_e^A)}{L}\begin{pmatrix} 1 & 0 & -1 & 0 \\ 0 & 0 & 0 & 0 \\ -1 & 0 & 1 & 0 \\ 0 & 0 & 0 & 0 \end{pmatrix}, \tag{3}$$

$$\mathbf{M}_e(x_e^M, x_e^A) = \frac{\rho(x_e^M)A_(x_e^A)L}{6}\begin{pmatrix} 2 & 0 & 1 & 0 \\ 0 & 2 & 0 & 1 \\ 1 & 0 & 2 & 0 \\ 0 & 1 & 0 & 2 \end{pmatrix}, \tag{4}$$

where $E(x_e^M)$, $\rho(x_e^M)$ and $A(x_e^A)$ are the interpolated values.

Following the methodology presented by Langlet et al. (1995), (1) is employed to ensure the infinite periodicity of the unit cell. For 2D problems, the wave vector $\mathbf{k}$ can be written as:

$$\mathbf{k} = ksin\theta\hat{I} + kcos\theta\hat{J} \tag{5}$$

where k is the length and θ is the angle relative to the horizontal direction. This vector moves around the IBZ perimeter. Thus, using Fig. 4 as reference, periodic Bloch

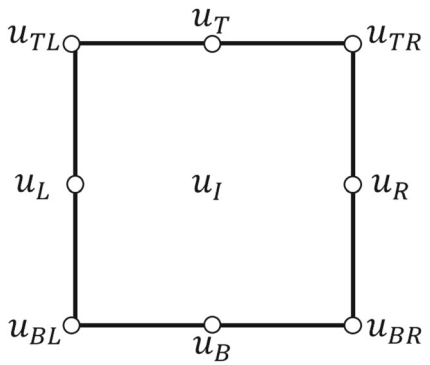

Fig. 4 Regions considered to impose periodicity in the unit cell

boundary conditions can be imposed according to the following relations:

$$\begin{aligned}
\mathbf{u}_T &= \mathbf{u}_B e^{iLkcos\theta} \\
\mathbf{u}_R &= \mathbf{u}_L e^{iLksin\theta} \\
\mathbf{u}_{BR} &= \mathbf{u}_{BL} e^{iLkcos\theta} \\
\mathbf{u}_{TL} &= \mathbf{u}_{BL} e^{iLksin\theta} \\
\mathbf{u}_{TR} &= \mathbf{u}_{BL} e^{iLk(cos\theta+sin\theta)}
\end{aligned} \tag{6}$$

where vector $\mathbf{u}_L$ represents all the nodes in the left line, $\mathbf{u}_R$ right line, $\mathbf{u}_B$ bottom line, and $\mathbf{u}_T$ top line. However, those vectors do not consider the corners, which are denoted by $\mathbf{u}_{BL}, \mathbf{u}_{BR}, \mathbf{u}_{TL}$, and $\mathbf{u}_{TR}$. All the internal nodes are arranged in the vector $\mathbf{u}_I$.

Thus, the number of independent nodes can be reduced with the relation $\mathbf{u} = \mathbf{T}\tilde{\mathbf{u}}$, where $\mathbf{u}$ is the vector of all nodal displacement, $\tilde{\mathbf{u}}$ is the reduced vector, and $\mathbf{T}$ is a matrix mapping both vectors. Vectors $\mathbf{u}$ and $\tilde{\mathbf{u}}$ are expressed as:

$$\mathbf{u} = \begin{bmatrix} \mathbf{u}_L \\ \mathbf{u}_R \\ \mathbf{u}_B \\ \mathbf{u}_T \\ \mathbf{u}_{BL} \\ \mathbf{u}_{TL} \\ \mathbf{u}_{BR} \\ \mathbf{u}_{TR} \\ \mathbf{u}_I \end{bmatrix}; \quad \tilde{\mathbf{u}} = \begin{bmatrix} \mathbf{u}_L \\ \mathbf{u}_B \\ \mathbf{u}_{BL} \\ \mathbf{u}_I \end{bmatrix}, \tag{7}$$

and matrix $\mathbf{T}$ is given by

$$\mathbf{T} = \begin{bmatrix} \mathbf{I} & 0 & 0 & 0 \\ \mathbf{I}e^{iLksin\theta} & 0 & 0 & 0 \\ 0 & \mathbf{I} & 0 & 0 \\ 0 & \mathbf{I}e^{iLkcos\theta} & 0 & 0 \\ 0 & 0 & \mathbf{I} & 0 \\ 0 & 0 & \mathbf{I}e^{iLksin\theta} & 0 \\ 0 & 0 & \mathbf{I}e^{iLkcos\theta} & 0 \\ 0 & 0 & \mathbf{I}e^{iLk(sin\theta+cos\theta)} & 0 \\ 0 & 0 & 0 & \mathbf{I} \end{bmatrix}. \tag{8}$$

With these basic definitions, it is possible to write the classical eigenvalue problem to take periodicity into account

$$\begin{aligned}
&\left(\mathbf{T}^T\mathbf{K}\mathbf{T} - \omega_i^2\mathbf{T}^T\mathbf{M}\mathbf{T}\right)\mathbf{u}_i = \mathbf{0}, \\
&\text{or} \\
&\left(\mathbf{K}'(\mathbf{k}) - \omega_i^2\mathbf{M}'(\mathbf{k})\right)\mathbf{u}_i = \mathbf{0},
\end{aligned} \tag{9}$$

where $\mathbf{K}$ and $\mathbf{M}$ are the global stiffness and mass matrices, respectively, λ_i corresponds to the ith eigenvalue ($\lambda_i = \omega_i^2$), and $\mathbf{u_i}$ the ith mode shape associated with the corresponding wave vector.

The periodic mapping matrix $\mathbf{T}$ introduces the dependence with respect to the wave vector $\mathbf{k}$ in the problem. Thus, if m eigenvalues are evaluated as a function of the wave vector and arranged along the path $\Gamma - M - X - \Gamma$, it is possible to plot a band diagram. This diagram characterizes the dynamic response of the microstructure as a function of $\mathbf{k}$ and shows what wavelengths can be transmitted along the unit cell.

4 Optimization problem

4.1 Optimization

The optimization problem consists of finding the microstructure that maximizes the band gap defined as the distance between two adjacent bands n and $n+1$. Figure 5 shows a typical band diagram with six bands (blue lines), where a gap between the third and fourth bands can be observed. The band gap width, which will be maximized, is defined as the distance between the minimum value of $\boldsymbol{\omega}_{n+1}(\mathbf{k})$, and the maximum value of $\boldsymbol{\omega}_n(\mathbf{k})$ for $\mathbf{k} \in [\Gamma, X, M, \Gamma]$. As previously defined, design variables $\mathbf{x}$ include the area x_e^A and material x_e^M of each element e and the wave vector $\mathbf{k}$ is evaluated at the perimeter of the IBZ. The formulation reads:

$$\max_{\mathbf{x}} \quad \min \boldsymbol{\omega}_{n+1}(\mathbf{x}, \mathbf{k}) - \max \boldsymbol{\omega}_n(\mathbf{x}, \mathbf{k}) \tag{10a}$$

$$\text{subject to} \quad (\mathbf{K}'(\mathbf{k}) - \omega^2\mathbf{M}'(\mathbf{k}))\mathbf{u} = \mathbf{0} \tag{10b}$$

$$0 \leq \mathbf{x}_i \leq 1 \tag{10c}$$

An issue when directly addressing eigenvalues in optimization is the non-differentiability associated with repeated eigenvalues. Another problem when targeting specific eigenvalues is the mode switch that may occur during optimization. Aiming to solve this problem, we propose the use of P-norm smooth approximations for both $\max \boldsymbol{\omega}_n$ and $\min \boldsymbol{\omega}_{n+1}$ in the form:

$$\max \boldsymbol{\omega}_n(\mathbf{k}) \approx \|\boldsymbol{\omega}_n\|_P = \left(\sum_{j=1}^{n}\sum_{i=1}^{IBZ}\omega_{ij}^P\right)^{1/P}, \tag{11}$$

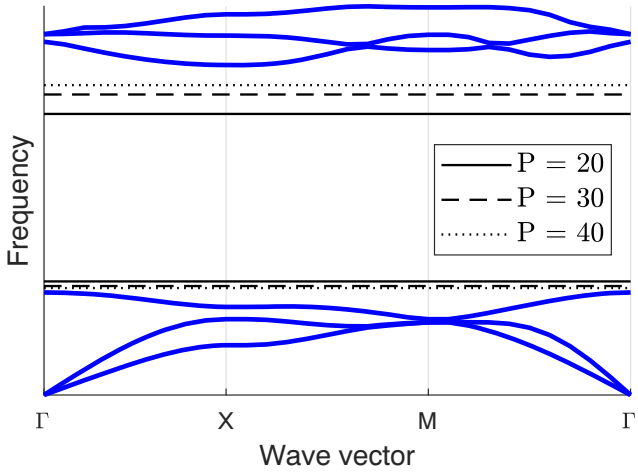

Fig. 5 Example of P-norm smooth approximations to minimum and maximum values of frequency, for $n = 3$ and $m = 6$

and

$$\min \boldsymbol{\omega}_{n+1}(\mathbf{k}) \approx \|\boldsymbol{\omega}_{n+1}\|_{-P} = \left(\sum_{j=n+1}^{m} \sum_{i=1}^{IBZ} \omega_{ij}^{-P} \right)^{-1/P}. \quad (12)$$

In both expressions, the sum $i = 1$ to IBZ is the discretization of the wave vector $\mathbf{k}$ and index j represents the band number.

In (11), the sum goes from $i = 1$ to n, representing the maximum value for bands 1 to n, that is, all the eigenvalues in this range are taken into account to evaluate the norm. Equation (12) considers all the eigenvalues from $n + 1$ to m, representing the minimum value for bands $n + 1$ to m. Both approximations combine a finite set of eigenvalues, thus hindering mode switch inside each set. Also, as the objective is to increase the distance between both sets, there is little possibility of mode switching between both sets, as discussed in the "Results" section. The non-differentiability is also not an issue, as discussed in Torii and De Faria (2017).

Figure 5 shows a band diagram containing a band gap. Equations (11) and (12) are evaluated considering $n = 3$ and $m = 6$ for different values of P. It can be seen that as P increases, (12) converges to the true minimum and (11) to the true maximum, even though there are intersections (repeated values) in the diagram.

4.2 Sensitivity analysis

The derivatives of (11) and (12) with respect to a design variable x_m^α are given by

$$\frac{d\|\boldsymbol{\omega}_n\|_P}{dx_m^\alpha} = \left(\sum_{j=1}^{n} \sum_{i=1}^{IBZ} \omega_{ij}^{P} \right)^{\frac{1-P}{P}} * \left(\sum_{j=1}^{n} \sum_{i=1}^{IBZ} \omega_{ij}^{P-1} \frac{d\omega_{ij}}{dx_m^\alpha} \right), \quad (13)$$

and

$$\frac{d\|\boldsymbol{\omega}_{n+1}\|_{-P}}{dx_{m^\alpha}} = \left(\sum_{j=n+1}^{m} \sum_{i=1}^{IBZ} \omega_{ij}^{-P} \right)^{\frac{-(1+P)}{P}} * \left(\sum_{j=n+1}^{m} \sum_{i=1}^{IBZ} \omega_{ij}^{-P-1} \frac{d\omega_{ij}}{dx_m^\alpha} \right), \quad (14)$$

where α can be either A (geometry) or M (material).

As presented by Haftka and Zafer (1992) the eigenvalue sensitivities are

$$\frac{d\omega_{ij}}{dx_m^\alpha} = \frac{u_{ij}^T \left(\frac{dK}{dx_m^\alpha} - \omega_{ij}^2 \frac{dM}{dx_m^\alpha} \right) u_{ij}}{2\omega_{ij} u_{ij}^T M u_{ij}}. \quad (15)$$

There is a subtle difference between differentiating with respect to x_m^A or x_m^M, due to the interpolation function defined in (2). The stiffness and mass matrices derivatives for both cases are given by

$$\frac{dK_e}{dx_m^A} = \frac{E(x_e^M)}{L} \frac{dA(x_e^A)}{dx_m^A} \begin{pmatrix} 1 & 0 & -1 & 0 \\ 0 & 0 & 0 & 0 \\ -1 & 0 & 1 & 0 \\ 0 & 0 & 0 & 0 \end{pmatrix} = \delta_{em} \frac{E(x_e^M)}{L} (A_2 - A_1) \begin{pmatrix} 1 & 0 & -1 & 0 \\ 0 & 0 & 0 & 0 \\ -1 & 0 & 1 & 0 \\ 0 & 0 & 0 & 0 \end{pmatrix}, \quad (16)$$

$$\frac{dM_e}{dx_m^A} = \frac{\rho(x_e^M)L}{6} \frac{dA(x_e^A)}{dx_m^A} \begin{pmatrix} 2 & 0 & 1 & 0 \\ 0 & 2 & 0 & 1 \\ 1 & 0 & 2 & 0 \\ 0 & 1 & 0 & 2 \end{pmatrix} = \delta_{em} \frac{\rho(x_e^M)L}{6} (A_2 - A_1) \begin{pmatrix} 2 & 0 & 1 & 0 \\ 0 & 2 & 0 & 1 \\ 1 & 0 & 2 & 0 \\ 0 & 1 & 0 & 2 \end{pmatrix}, \quad (17)$$

$$\frac{dK_e}{dx_m^M} = \frac{A(x_e^A)}{L} \frac{E(x_e^M)}{dx_m^M} \begin{pmatrix} 1 & 0 & -1 & 0 \\ 0 & 0 & 0 & 0 \\ -1 & 0 & 1 & 0 \\ 0 & 0 & 0 & 0 \end{pmatrix} = \delta_{em} \frac{A(x_e^M)}{L} (E_2 - E_1) \begin{pmatrix} 1 & 0 & -1 & 0 \\ 0 & 0 & 0 & 0 \\ -1 & 0 & 1 & 0 \\ 0 & 0 & 0 & 0 \end{pmatrix}, \quad (18)$$

and

$$\frac{dM_e}{dx_m^M} = \frac{A(x_e^A)L}{6} \frac{d\rho(x_e^M)}{dx_m^M} \begin{pmatrix} 2 & 0 & 1 & 0 \\ 0 & 2 & 0 & 1 \\ 1 & 0 & 2 & 0 \\ 0 & 1 & 0 & 2 \end{pmatrix} = \delta_{em} \frac{A(x_e^A)L}{6} (\rho_2 - \rho_1) \begin{pmatrix} 2 & 0 & 1 & 0 \\ 0 & 2 & 0 & 1 \\ 1 & 0 & 2 & 0 \\ 0 & 1 & 0 & 2 \end{pmatrix}, \quad (19)$$

where δ_{em} denotes the Kronecker's delta.

5 Results

The "Results" section will be divided into three parts. First, the parameters of the optimization algorithm are set, then the use of P-norm as a formulation to avoid the non-differentiability problem of repeated eigenvalues is analyzed and the optimization convergence is studied. Finally, the optimization is performed to obtain the optimal lattices and band diagrams for different values of n_c.

5.1 Optimization settings

Parameters such as areas, mechanical properties, and dimensions are shown in Table 1. Density and Young's modulus are represented by ρ and E respectively, where the sub-index 1 is for aluminum and 2 for tungsten. These base materials are used to allow a large contrast in material properties.

Cross-section is assumed circular, with limit diameters $D_1 = 0.004[m]$ and $D_2 = 0.008[m]$, respectively. Also, the length of the basic cell L_b (shown in Fig. 1a) is set to $0.025[m]$. Target bands are $n = 3$ (lower band) and $n+1 = 4$ (upper band). Thus, the objective is to maximize the band gap between the respective frequencies for all wave vectors, as stated in (10a). The wave vector discretization consists of 30 evenly spaced points. It should be noted that an underestimation of the number of points could result in a miscalculation of the band gap. Thus, a careful investigation is recommended for other problems.

The band gap maximization is a non-convex problem; thus, different starting points give different optimal solutions. To overcome this problem, the Latin hyper-cube sampling method (Iman et al. 1980) is used to obtain near-random initial samples in the search space. One hundred different initial points are used to evaluate the reference problem (no smooth approximation). This set of initial design variables is used as the starting point for all other problems in the rest of this manuscript. This procedure is employed to guarantee that the results presented herein are always compared to the best solution of the reference formulation.

The optimization is performed using the Method of Moving Asymptotes (MMA) (Svanberg 1987) and Globally Convergent Method of Moving Asymptotes (GCMMA) (Svanberg 2002). MMA is initially used to verify the stability of the optimization procedure with both the reference formulation and the proposed formulation. As some oscillations are observed, especially in the reference formulation, GCMMA is employed to obtain the optimized structures and band gaps in the rest of the manuscript. Default values were used for both MMA and GCMMA, as provided by Prof. Krister Svanberg (2007).

Although the use of base materials with a large contrast in material properties usually leads to 0/1 designs in band gap optimization, sometimes it is necessary to post-process the optimized solution. As the obtained solutions are almost 0/1, it is employed the direct rounding for the nearest value whenever a post-processed result is presented. The same is performed to cross-section results, even though intermediate cross-sections are allowed.

Table 1 Parameters used in this work

Parameter	Value	Dimension
E_1	70	[GPa]
ρ_1	2.7×10^3	[kg/m^3]
E_2	411	[GPa]
ρ_2	19.3×10^3	[kg/m^3]
A_1	$4\pi \times 10^{-6}$	[m^2]
A_2	$16\pi \times 10^{-6}$	[m^2]
L_b	2.5×10^{-2}	[m]

5.2 P-Norm analysis

Problems associated with sensitivity of eigenvalues are analyzed by comparing the traditional formulation to the proposed approach. Traditional formulation is denoted by $P = \infty$ for consistency with the proposed formulation. The analysis is performed for different values of P and different numbers of basic cells n_c. In this study, the MMA algorithm is used to study the behavior of both the reference and proposed formulation, since instabilities in sensitivity imply oscillations in the convergence behavior. Gravesen et al. (2011) discuss the appearance of peaks in the eigenvalues and, consequently, oscillations in the objective function during the optimization process, due to repeated eigenvalues. This behavior leads to difficult or even no convergence of the optimization procedure. Figure 6 shows the results obtained using $n_c = 6$ with $P = 10, 20, 30, 40,$ and ∞.

As can be seen in the convergence curves depicted in Fig. 6, the reference formulation ($P = \infty$) shows strong oscillations in the first iterations when compared to the proposed formulation. Other interesting results obtained from the convergence curves are the faster convergence when using the proposed formulation (due to fewer oscillations) and the convergence to the reference band gap value as exponent P increases. Oscillations in the final iterations are expected when using MMA, but as can be seen in the curves, the oscillation steadily decreases when using the proposed formulation. Another remarkable difference is the amount of variation since for $P = \infty$ the variation is on the second decimal digit whereas the variation is on the fourth digit or less when using the proposed formulation.

GCMMA is then used in the rest of this manuscript since it is better suited to deal with oscillations due to its

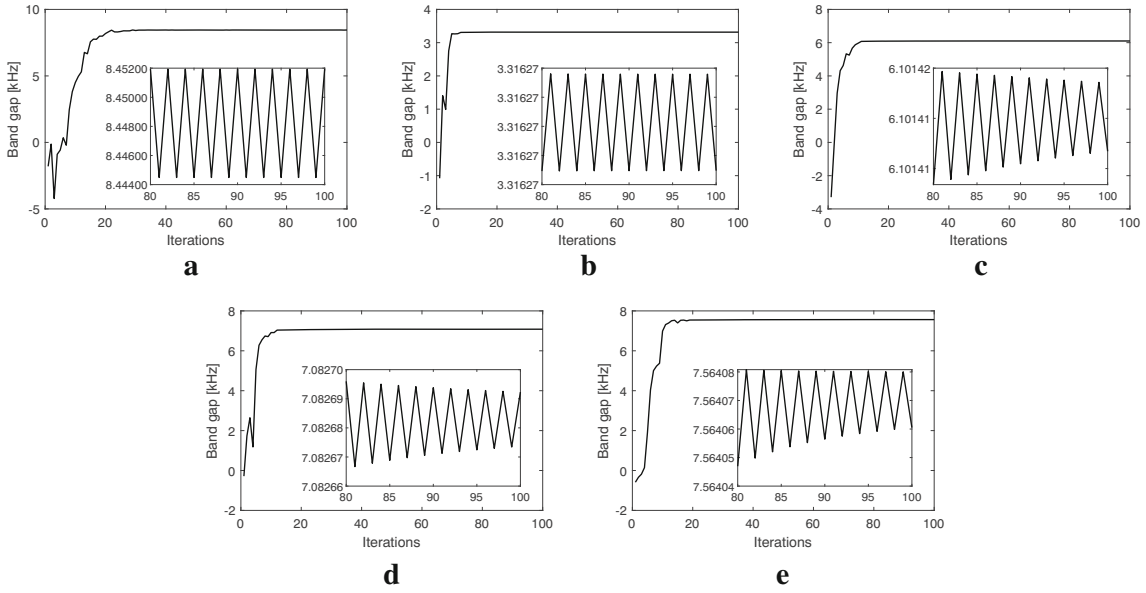

Fig. 6 Convergence plots obtained for $n_c = 6$ with the reference and with the proposed formulation for different P exponents and MMA optimizer. **a** Reference formulation ($P = \infty$). **b** P = 10. **c** P = 20. **d** P = 30. **e** P = 40

conservative nature. Figure 7 shows the convergence plots of the objective function through the outer iterations of the GCMMA for different exponents P and different number of base cells n_c.

The optimization with any finite value of P reaches the maximum before and more smoothly when compared to the reference formulation ($P = \infty$). Again, convergence to the reference band gap is obtained as exponent P increases. Although the convergence plots depicted in Fig. 7 show less oscillation when compared to the convergence plots shown in Fig. 6, it is also important to investigate the number of inner iterations used during each outer iteration. Figure 8 shows the remarkable difference in the number of inner iterations between the reference formulation and the proposed formulation for all exponents studied in this work and $n_c = 6$.

Both unprocessed and post-processed band gap values are presented in Table 2, for different values of n_c and P. In this work, values of P from 10 to 40 resulted in similar unprocessed band gaps. Torii and Faria (2017) considered

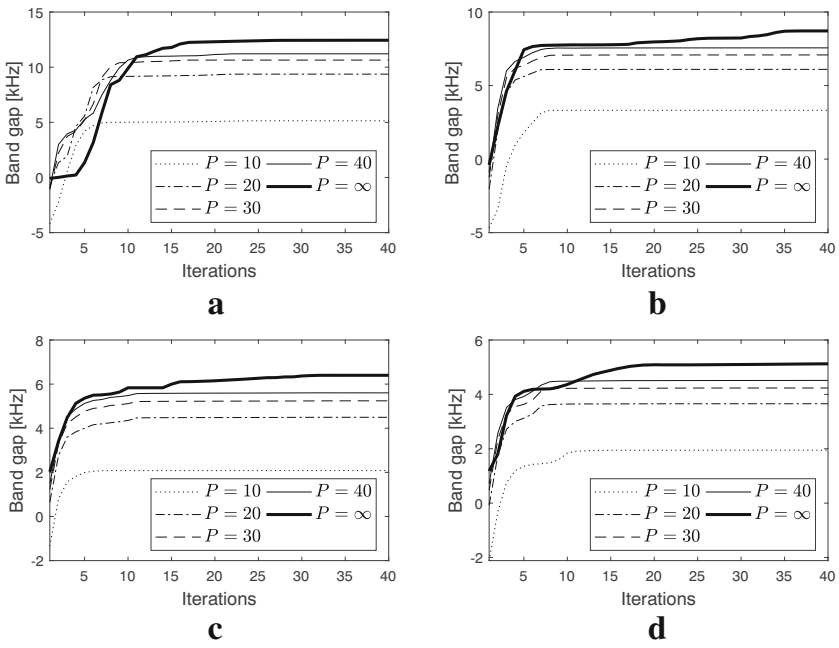

Fig. 7 Convergence curves of the objective function trough the outer iterations of GCMMA for different values of exponent P and number of base cells n_c. **a** nc = 4. **b** nc = 6. **c** nc = 8. **d** nc = 10

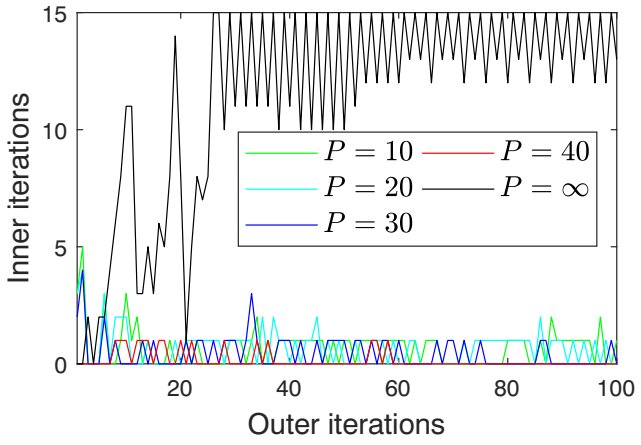

Fig. 8 Number of inner iterations of the GCMMA method for each outer iteration of Fig. 7 (**b**)

values between 5 and 20 when using the P-norm for the maximization of eigenvalues in topology optimization, with good results. Thus, it seems that the main difference observed in these results is the influence of P in the post -processed results.

Also, for a small number of variables ($n_c = 4$), the same post-processed result is obtained independent of P and for a larger number of variables, a larger P resulted in the best post-processed results (the best results are highlighted in Table 2, for each n_c). It should also be stressed that large values of P provide a better approximation for the objective function, but also increase the degree of nonlinearity of the objective function, such that a good compromise should be considered.

5.3 Optimized band gap and lattice

In this section, the optimum solution and the corresponding band diagrams are presented for a different number of basic cells n_c. The best solutions highlighted in Table 2 are used herein.

The optimized lattice configurations are presented in Fig. 9. Each bar is shown as a red line for tungsten and as a blue line for aluminum. Cross-sections are represented by the relative thickness of each line.

It can be seen the predominance of thick tungsten bars at the corners and thin aluminum bars in the rest of the lattice. A similar behavior was reported in band gap optimization of 2D problems when two different materials are used (Sigmund and Søndergaard Jensen 2003; Yi et al. 2019).

Figure 10 shows the band diagrams corresponding to the lattices shown in Fig. 9. To make a comparative analysis, Table 3 presents the central frequency for the corresponding band gap, the absolute band gap value, and the relative band gap, defined as the ratio of the absolute band gap and the

Table 2 Optimized values for the band gap [kHz] in function of both number of cells n_c and exponent P

$\mathbf{n_c}$	P	Band gap without post-processing [kHz]	Band gap with post-processing [kHz]
	$P = 10$	12.387	12.367
	$P = 20$	12.384	12.367
4	$P = 30$	12.401	12.367
	$P = 40$	12.416	12.367
	$P = \infty$	12.446	12.367
	$P = 10$	8.252	8.183
	$P = 20$	8.615	8.390
6	$P = 30$	8.680	7.903
	$P = 40$	8.709	7.795
	$P = \infty$	8.715	7.963
	$P = 10$	5.574	5.418
	$P = 20$	6.374	6.290
8	$P = 30$	6.439	6.374
	$P = 40$	6.457	6.374
	$P = \infty$	6.403	6.144
	$P = 10$	4.962	4.902
	$P = 20$	5.095	5.062
10	$P = 30$	5.122	5.038
	$P = 40$	5.133	5.091
	$P = \infty$	5.124	4.889

Both unprocessed and post-processed values are presented and the best post-processed solutions are highlighted

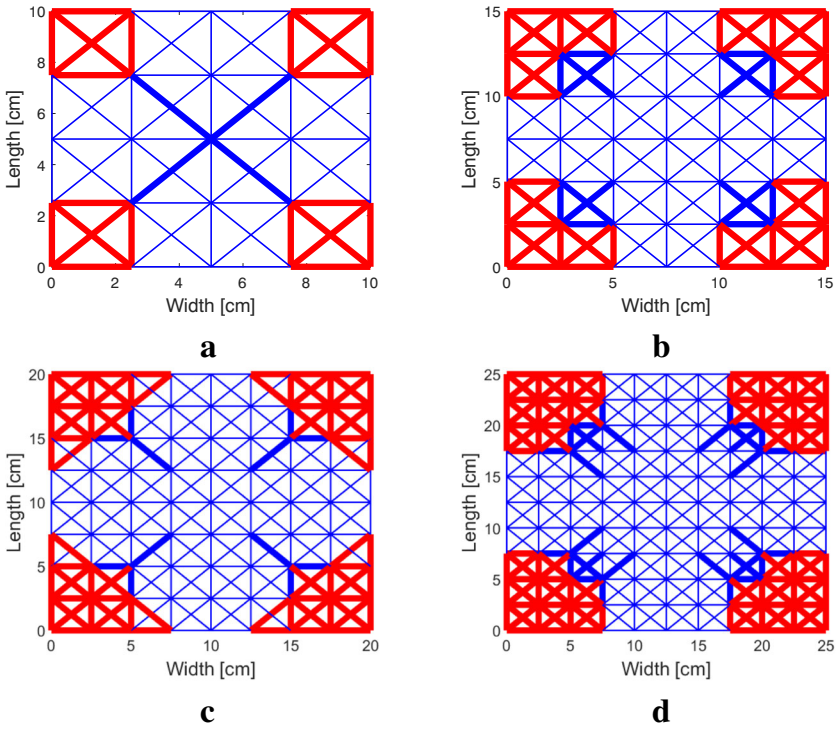

Fig. 9 Optimized lattices obtained for different number of base cells n_c. Thickness of line denotes the relative cross-section value. Line colors denote base material (red for tungsten and blue for aluminum). **a** nc = 4. **b** nc = 6. **c** nc = 8. **d** nc = 10

central frequency. In all cases, the relative band gap is close to 1.0, such that increasing the number of cells does not necessarily lead to an improvement. The only effect that can be observed when increasing the number of cells is a reduction in the mean band gap frequency. This effect can be explained by the fact that the size of the microstructure is a multiple of L_b, such that increasing n_c results in a larger unit cell. Also, as the number of degrees of freedom increases and we are always considering $n = 3$, there is a tendency of targeting a lower central band gap frequency. Thus, a simpler lattice with $n_c = 4$ performs as well as a lattice with $n_c = 10$, unless lower frequencies are targeted.

The relative band gap obtained with truss-like structures results in a large improvement compared to some results presented in other studies using plane elasticity. Examples of relative band gap values found in the literature are 0.45 (Yi et al. 2019) and 0.65 (Dong et al. 2014a). Li et al. (2016) obtained larger values, in the order of 1.0, for complex

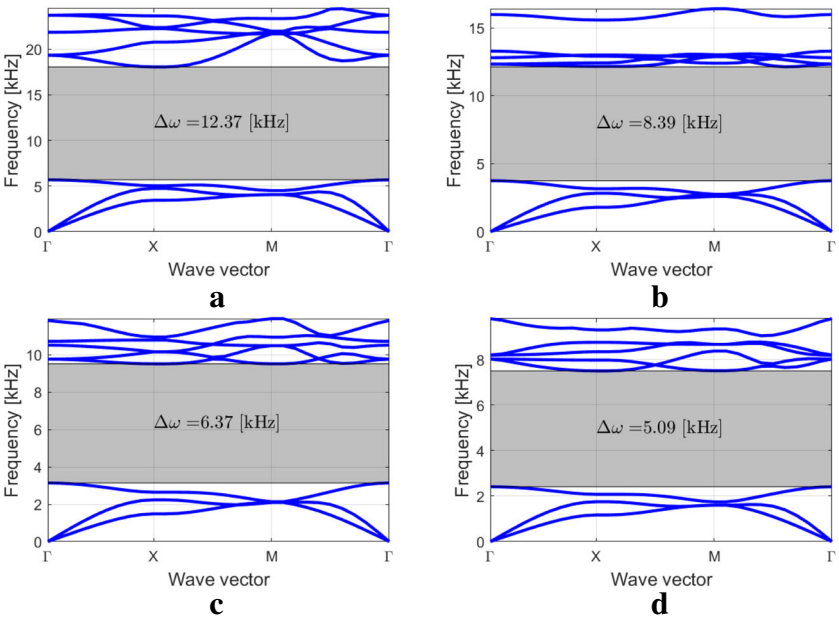

Fig. 10 Optimized band diagram for the lattices shown in Fig. 9. **a** nc = 4. **b** nc = 6. **c** nc = 8. **d** nc = 10

Table 3 Central frequency in which the band gap is tuned, absolute and relative band gap [kHz] with respect to the number of cells n_c

$\mathbf{n_c}$	Relative band gap [kHz]	Central frequency [kHz]	Absolute band gap [kHz]
4	1.042	11.865	12.367
6	1.054	7.954	8.390
8	1.007	6.326	6.374
10	1.026	4.958	5.091

2D structures. This contrasts with our results with relative band gaps in the order of 1.0 but obtained with a simpler formulation (truss), showing that with this type of structures wide band gaps can be achieved.

In addition to the previous analysis, it is worth mentioning that the bands in the diagram of Fig. 10 include plenty of points with the same frequency for a given wave vector. For example, it is possible to verify the intersection of at least 3 bands at point M, indicating repeated eigenvalues.

6 Concluding remarks

In this article, the possibility of optimizing ultra-light cellular truss structure with the ability to conceive large phononic band gaps was investigated. Each element of the periodic lattice has two design variables, the first related to the cross-sectional area whereas the second variable is associated with the material. To handle the non-differentiation of repeated eigenvalues as well as problems associated with mode switch, a new method based on the P-norm is proposed. The methodology was evaluated using 2D truss-like structures with different levels of complexity.

The results show that the P-norm contributes to a smoother and faster optimization convergence. Furthermore, better solutions (wider band gaps) were obtained when the P-norm was implemented and the results are post-processed. It was also demonstrated that the relative band gap obtained with truss-like structures results in improvement compared to the results presented in other studies using 2D solid elements.

Finally, an increment in the number of basic cells n_c (related to the lattice complexity) is not justified, since the improvements in the relative band gap width were not observed for the problems studied herein. Also, simpler structures are desirable to simplify the manufacturing process. More complex structures (a larger number of base cells) may be justified only if lower frequencies are needed, as the mass of the model is increased.

Acknowledgements The authors would like to thank Professor Krister Svanberg for providing the GCMMA and MMA codes.

Funding The authors received financial support provided by the Millennium Science Initiative of the Ministry of Economy, Development and Tourism, grant "Millennium Nucleus on Smart Soft Mechanical Metamaterials" and the financial support from the Santa Catarina State Research Founding Agency (FAPESC process number: 2019TR779).

Compliance with ethical standards

Conflict of interest The authors declare that they have no conflict of interest.

Replication of results The authors state that all the data necessary to replicate the results are presented in the manuscript.

References

Bathe K-J (2006) Finite element procedures. Klaus-Jurgen Bathe

Bendsøe MP, Sigmund O (1999) Material interpolation schemes in topology optimization. Arch Appl Mech 69(9-10):635–654

Bendsøe MP, Sigmund O (2003) Topology optimization: theory, methods and applications. Springer, Berlin

Bilal OR, Hussein MI (2011a) Ultrawide phononic band gap for combined in-plane and out-of-plane waves. Phys Rev E 84(6):065701

Bilal OR, Hussein MI (2011b) Optimization of phononic crystals for the simultaneous attenuation of out-of-plane and in-plane waves. In: ASME 2011 International mechanical engineering congress and exposition. American Society of Mechanical Engineers, pp 969–972

Brillouin L (1953) Wave propagation in periodic structures: electric filters and crystal lattices. Dover Publications Inc

Cheung KC, Gershenfeld N (2013) Reversibly assembled cellular composite materials. Science 341(6151):1219–1221

Cramer NB, Cellucci DW, Formoso OB, Gregg CE, Jenett BE, Kim JH, Lendraitis M, Swei SS, Trinh GT, Trinh KV, et al. (2019) Elastic shape morphing of ultralight structures by programmable assembly. Smart Mater Struct 28(5):055006

Diaz A, Haddow A, Ma L (2005) Design of band-gap grid structures. Struct Multidiscip Optim 29(6):418–431

Dong H-W, Su X-X, Wang Y-S (2014a) Multi-objective optimization of two-dimensional porous phononic crystals. Journal of Physics D: Applied Physics 47(15):155301

Dong H-W, Su X-X, Wang Y-S, Zhang C (2014b) Topology optimization of two-dimensional asymmetrical phononic crystals. Phys Lett A 378(4):434–441

Gazonas GA, Weile DS, Wildman R, Mohan A (2006) Genetic algorithm optimization of phononic bandgap structures. Int J Solids Struct 43(18-19):5851–5866

Gravesen J, Evgrafov A, Nguyen DM (2011) On the sensitivities of multiple eigenvalues. Structural and Multidisciplinary optimization 44(4):583–587

Haftka RT, Zafer G (1992) Elements of structural optimization. Kluwer Academic Publ

Halkjær S, Sigmund O, Jensen JS (2005) Inverse design of phononic crystals by topology optimization. Zeitschrift für Kristallographie-Crystalline Materials 220(9-10):895–905

Halkjær S, Sigmund O, Jensen JS (2006) Maximizing band gaps in plate structures. Struct Multidiscip Optim 32(4):263–275

Hedayatrasa S, Abhary K, Uddin M, Guest JK (2016) Optimal design of tunable phononic bandgap plates under equibiaxial stretch. Smart Mater Struct 25(5):055025

Hedayatrasa S, Abhary K, Uddin M, Ng C-T (2016) Optimum design of phononic crystal perforated plate structures for widest bandgap of fundamental guided wave modes and maximized in-plane stiffness. Journal of the Mechanics and Physics of Solids 89:31–58

Hussein MI, Hamza K, Hulbert GM, Saitou K (2007) Optimal synthesis of 2d phononic crystals for broadband frequency isolation. Waves Random Complex Media 17(4):491–510

Hussein MI, Leamy MJ, Ruzzene M (2014) Dynamics of phononic materials and structures: historical origins, recent progress, and future outlook. Appl Mech Rev 66(4):040802

Iman R, Davenport J, Zeigler D (1980) Latin hypercube sampling (program user's guide). [lhc, in fortran] 1

Jensen JS (2003) Phononic band gaps and vibrations in one-and two-dimensional mass–spring structures. J Sound Vib 266(5):1053–1078

Kittel C, McEuen P (1996) Introduction to solid state physics, vol 8. Wiley, New York

Langlet P, Hladky-Hennion A-C, Decarpigny J-N (1995) Analysis of the propagation of plane acoustic waves in passive periodic materials using the finite element method. The Journal of the Acoustical Society of America 98(5):2792–2800

Li X-S, Fang S-C (1997) On the entropic regularization method for solving min-max problems with applications. Mathematical Methods of Operations Research 46(1):119–130

Li Y, Huang X, Meng F, Zhou S (2016) Evolutionary topological design for phononic band gap crystals. Struct Multidiscip Optim 54(3):595–617

Li Y, Huang X, Zhou S (2016) Topological design of cellular phononic band gap crystals. Materials 9(3):186

Liebold-Ribeiro Y, Körner C (2014) Phononic band gaps in periodic cellular materials. Adv Eng Mater 16(3):328–334

Liu S., Cao X. (2006) Design of band-gaps of truss-like materials by size optimization. In: China-japan-korea Joint Symposium on Optimization of Structural & Mechanical Systems, pp 635–640

Liu Z-F, Wu B, He C-F (2014) Band-gap optimization of two-dimensional phononic crystals based on genetic algorithm and fpwe. Waves Random Complex Media 24(3):286–305

Ruzzene M, Scarpa F (2005) Directional and band-gap behavior of periodic auxetic lattices. Physica Status Solidi (B) 242(3):665–680

Schaedler TA, Carter WB (2016) Architected cellular materials. Annu Rev Mater Res 46:187–210

Seyranian AP, Lund E, Olhoff N (1994) Multiple eigenvalues in structural optimization problems. Structural Optimization 8(4):207–227

Sigmund O, Søndergaard Jensen J (2003) Systematic design of phononic band–gap materials and structures by topology optimization. Philosophical Transactions of the Royal Society of London. Series A: Mathematical, Phys Eng Sci 361(1806):1001–1019

Svanberg K (1987) The method of moving asymptotes—a new method for structural optimization. Int J Numer Methods Eng 24(2):359–373

Svanberg K (2002) A class of globally convergent optimization methods based on conservative convex separable approximations. SIAM J Optim 12(2):555–573

Svanberg K (2007) Mma and gcmma-two methods for nonlinear optimization

Torii AJ, De Faria JR (2017) Structural optimization considering smallest magnitude eigenvalues: a smooth approximation. J Braz Soc Mech Sci Eng 39(5):1745–1754

Vatanabe SL, Paulino GH, Silva EC (2014) Maximizing phononic band gaps in piezocomposite materials by means of topology optimization. The Journal of the Acoustical Society of America 136(2):494–501

Vatanabe SL, Silva EC (2011) Design of phononic band gaps in functionally graded piezocomposite materials by using topology optimization. In: Behavior and mechanics of multifunctional materials and composites 2011, vol 7978. International Society for Optics and Photonics, p 797811

Wang P, Casadei F, Kang SH, Bertoldi K (2015) Locally resonant band gaps in periodic beam lattices by tuning connectivity. Phys Rev B 91(2):020103

Warmuth F, Körner C (2015) Phononic band gaps in 2d quadratic and 3d cubic cellular structures. Materials 8(12):8327–8337

Yi G, Shin YC, Yoon H, Jo S-H, Youn BD (2019) Topology optimization for phononic band gap maximization considering a target driving frequency. JMST Advances 1(1-2):153–159

Yi G, Youn BD (2016) A comprehensive survey on topology optimization of phononic crystals. Struct Multidiscip Optim 54(5):1315–1344